arXiv:1304.4574v1 [quant-ph] 16 Apr 2013

Collectively-enhanced optomechanical coupling in periodic arrays of scatterers

André Xuereb,[1, 2, *] Claudiu Genes,[3, 4] and Aurélien Dantan[5]

[1] *Department of Physics, University of Malta, Msida MSD 2080, Malta*
[2] *Centre for Theoretical Atomic, Molecular and Optical Physics,*
School of Mathematics and Physics, Queen's University Belfast, Belfast BT7 1NN, United Kingdom
[3] *Institut für Theoretische Physik, Universität Innsbruck, Technikerstrasse 25, A-6020 Innsbruck, Austria*
[4] *ISIS (UMR 7006) and IPCMS (UMR 7504), Université de Strasbourg and CNRS, Strasbourg, France*
[5] *QUANTOP, Danish National Research Foundation Center for Quantum Optics,*
Department of Physics and Astronomy, University of Aarhus, 8000 Aarhus C, Denmark

(Dated: April 17, 2013)

In a recent publication [A. Xuereb, C. Genes, and A. Dantan, Phys. Rev. Lett. **109**, 223601 (2012)] the optomechanical properties of a periodic array of identical scatterers placed inside an optical cavity were investigated. It was shown that operating at a point where the array is transmissive results in a linear optomechanical coupling strength between the cavity field and a collective motional mode that may be several orders of magnitude stronger than is possible with an equivalent reflective ensemble. In this publication we describe and interpret these effects in significantly greater detail, investigate the nature of the scaling laws noted previously, and discuss their robustness to imperfections.

PACS numbers: 42.50.Wk, 07.10.Cm, 07.60.Ly, 42.79.Gn

The ability to measure and control the motion of massive mechanical oscillators has progressed dramatically in recent years [1, 2], and several important milestones have been reached in the field of optomechanics towards bringing this level into the quantum regime, including the cooling to the motional quantum ground state [3–5], the detection of quantized mechanical motion [6, 7], and the observation of the ponderomotive squeezing of light [8, 9] or of the radiation-pressure shot noise on a mechanical oscillator [10].

One challenge faced by the current generation of optomechanical experiments is that the interaction strength between a single photon and a single massive mechanical element is typically very weak. This can be ameliorated by confining light in wavelength-scale structures [11] or, generically, counteracted by the use of strong light fields in an optical resonator to amplify the interaction strength [12], albeit at the expense of trading off the intrinsically nonlinear nature of the radiation-pressure interaction (see, however, the recent proposals in Refs. [13, 14]). A growing number of theoretical proposals has contemplated the opposite – 'strong coupling' – regime, where a single photon can affect the motion of the oscillator significantly, thus giving access to the full quantum nature of the optomechanical interaction [15–23].

On the other hand, *collective* effects in optomechanical systems involving multiple mechanical and electromagnetic field modes have been discussed in a number of theoretical works, in connection with, e.g., optomechanical entanglement [24–34], enhanced displacement sensitivity [35–37], optomechanical nonlinearities [20, 21, 38–40], quantum information processing [41–44], many-body physics [45–49], as well as in a number of recent experiments [50–56]. Collective optomechanical effects are also at the heart of cavity optomechanics with cold atomic ensembles [57].

Motivated by the exploration of such collective optomechanical effects, we recently [58] showed that the collective motion of a periodic array of identical scatterers, when placed inside a cavity field, can couple very strongly to the optical field in the configuration where the array is *transmissive*, in contrast to the usual *reflective* optomechanics approach. The aim of the present work is to present a more detailed exploration of this system, to highlight the regimes in which these generic collective effects are seen, and to explore its robustness to imperfections.

This paper is organized as follows. In the next section we discuss the tools used to model a periodic array of N identical elements, and show that such an array can be modeled as a single effective element in the framework of the transfer matrix theory for one-dimensional scatterers. Section II discusses the optomechanical properties of such a generic N-element stack, when placed inside an optical cavity, in two distinct and opposite regimes: (i) A maximally-reflective stack (Sec. II B), and (ii) A transmissive stack (Sec. II C). We also show that the equations of motion for the system at hand are effectively described by an optical field interacting with a single collective mechanical mode. The next section discusses the second regime in further detail, and explores the scaling of the optomechanical coupling strength in the transmissive regime with the various system parameters; we show that the increase in the optomechanical coupling strength with the number of scatterers combines with an effect whereby the linewidth of the cavity resonance is narrowed due to the presence of the stack to provide an enhancement of the optomechanical cooperativity by sev-

---

[*] Corresponding author. andre.xuereb@qub.ac.uk

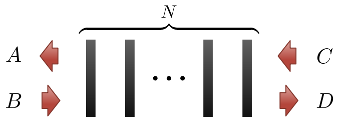

FIG. 1. Schematic diagram illustrating the basis of the model: N scatterers interacting with four running waves. B and C represent incident fields, A and D outgoing fields. The four field amplitudes are connected by means of transfer matrices.

eral orders of magnitude over that of a single element system. Section IV examines the robustness of these effects with respect to deviations from the ideal periodic array of identical, lossless scatterers, and Sec. V provides numerical estimates for the mechanisms we predict, based on state-of-the-art experiments.

I. MODELING AN N-ELEMENT STACK

Throughout this paper we shall restrict ourselves to a one-dimensional system and use the transfer matrix formalism to model a periodic N-element array, as illustrated in Fig. 1. As is well-known [59, 60], this formalism can treat elements ('scatterers') that interact linearly with the electromagnetic field, no matter the strength of this interaction or whether the scatterer is lossless or not. Within this formalism, each scatterer is parametrized by its polarizability ζ, which is real for lossless scatterers but complex in the presence of absorption. ζ is related to the amplitude reflectivity r of the element through the relation

$$r = \frac{i\zeta}{1 - i\zeta}\,, \tag{1}$$

and, for a lossless scatterer, we have

$$|r|^2 = \frac{\zeta^2}{1+\zeta^2}\,, \tag{2}$$

which allows us to link our results to, e.g., those in Ref. [61] through their Eq. (8). The flexibility afforded by the transfer matrix formalism allows us to treat ensembles of atoms in an optical lattice on the same footing as periodic arrays of macroscopic scattering elements (e.g., arrays of thin dielectric membranes) in the limit of a one-dimensional scattering theory, as we illustrate in App. A and App. B.

A. Transfer matrix for N-element stack

Let us consider N equally-spaced, identical and non-absorbing elements, each of which has a thickness much smaller than an optical wavelength. The spacing d between these elements determines the overall optical properties of the ensemble. Our starting point is the matrix that links the fields interacting with a single element of polarizability ζ [59],

$$M_{\mathrm{m}}(\zeta) \equiv \begin{bmatrix} 1+i\zeta & i\zeta \\ -i\zeta & 1-i\zeta \end{bmatrix}\,, \tag{3}$$

and the matrix that describes propagation of a monochromatic beam of wavenumber k over a distance d through free space,

$$M_{\mathrm{p}}(d) \equiv \begin{bmatrix} e^{ikd} & 0 \\ 0 & e^{-ikd} \end{bmatrix}\,, \tag{4}$$

both of which have unit determinant. These matrices relate forward- and backward-propagating electromagnetic waves on either side of the element:

$$\begin{pmatrix} A \\ B \end{pmatrix} = M \cdot \begin{pmatrix} C \\ D \end{pmatrix}\,, \tag{5}$$

where A and C (B and D) are the amplitudes of the backward- (forward-) propagating waves, as illustrated in Fig. 1. We wish to evaluate a product of the form

$$M_{\mathrm{m}}(\zeta) \cdot M_{\mathrm{p}}(d) \cdot M_{\mathrm{m}}(\zeta) \cdots M_{\mathrm{m}}(\zeta)\,, \tag{6}$$

with N copies of $M_{\mathrm{m}}(\zeta)$. First, we note that

$$\begin{aligned} &M_{\mathrm{p}}(d/2) \cdot M_{\mathrm{m}}(\zeta) \cdot M_{\mathrm{p}}(d) \cdots M_{\mathrm{m}}(\zeta) \cdot M_{\mathrm{p}}(d/2) \\ &\qquad = \left[M_{\mathrm{p}}(d/2) \cdot M_{\mathrm{m}}(\zeta) \cdot M_{\mathrm{p}}(d/2)\right]^N \equiv M^N\,, \end{aligned} \tag{7}$$

where the second line defines the matrix M:

$$M \equiv \begin{bmatrix} (1+i\zeta)e^{ikd} & i\zeta \\ -i\zeta & (1-i\zeta)e^{-ikd} \end{bmatrix}\,. \tag{8}$$

We can easily see that $\det M = 1$, whereby it can be shown [62] that for real ζ we can write

$$M^N = \begin{bmatrix} (1+i\chi)e^{i(kd+\mu)} & i\chi \\ -i\chi & (1-i\chi)e^{-i(kd+\mu)} \end{bmatrix}\,, \tag{9}$$

where $\chi \equiv \zeta U_{N-1}(a)$, with $U_n(x)$ being the n^{th} Chebyshev polynomial of the second kind, $a = \cos(kd) - \zeta\sin(kd)$, and

$$e^{i\mu} = \frac{1 - i\zeta U_{N-1}(a)}{(1-i\zeta)U_{N-1}(a) - e^{ikd}U_{N-2}(a)}\,. \tag{10}$$

Upon removing the padding of $d/2$ from either side, we obtain the matrix that describes the N-element ensemble:

$$M_N \equiv M_{\mathrm{p}}[\mu/(2k)] \cdot M_{\mathrm{m}}(\chi) \cdot M_{\mathrm{p}}[\mu/(2k)]\,. \tag{11}$$

In this respect, N lossless elements behave as a collective 'superelement' of polarizability χ along with a phase shift $\mu/2$ on either side of the stack.

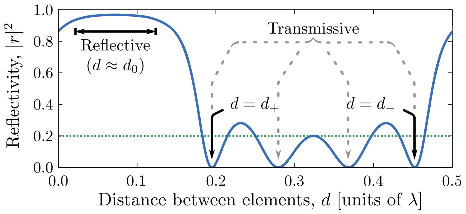

FIG. 2. Intensity reflectivity of $N = 5$ lossless elements, each of which has reflectivity 20% (shown as the dotted green line), as the spacing between the elements is scanned. We denote the inter-element distance where the reflectivity attains its peak as d_0, and two of the distances where the reflectivity is zero as $d_\pm$. The curve is periodic with period $\lambda/2$.

Let us note, finally, the link between the transfer matrix of any optical system and its amplitude transmissivity and reflectivity. Indeed, suppose we can describe a system by means of the transfer matrix

$$\begin{bmatrix} m_{11} & m_{12} \\ m_{21} & m_{22} \end{bmatrix} . \tag{12}$$

Then, the complex transmissivity of the system is simply

$$\mathcal{T} = \frac{1}{m_{22}} , \tag{13}$$

and the corresponding reflectivity

$$\mathcal{R} = \frac{m_{12}}{m_{22}} , \tag{14}$$

These quantities are used throughout this paper to characterize the optical properties of our system. A plot of the intensity reflectivity of a lossless 5-element ensemble as the spacing between pairs of elements is varied is shown in Fig. 2. Note that, despite each element having a reflectivity of 20%, the reflectivity of the entire ensemble ranges from 0% (e.g., at $d = d_\pm$) to about 97% (at $d = d_0$).

II. OPTOMECHANICS OF A PERIODIC ARRAY OF SCATTERERS

Our next task is to place the array just described inside a near-resonant optical cavity. The interaction of the array with the cavity field will shift the resonances of the main cavity. As is usual in optomechanics, we assume that each element in the array is harmonically trapped, and are interested in one particular figure of merit: the coupling strength equal to the frequency shift incurred by the cavity resonance when the array undergoes a displacement equal to the size of the relevant zero-point-fluctuations. As a yardstick we shall use the quantity

$$g \equiv \frac{2\omega_{\mathrm{c}} x_{\mathrm{zpt}}}{L} , \tag{15}$$

which is the optomechanical coupling strength for a perfectly reflective mirror near the center of a cavity of length L and resonant frequency ω_{c} [63]. The size of the zero-point-fluctuations of each element is denoted by $x_{\mathrm{zpt}} = \sqrt{\hbar/(m\omega_{\mathrm{m}})}$, where m is the effective mass of the element and ω_{m} its oscillation frequency.

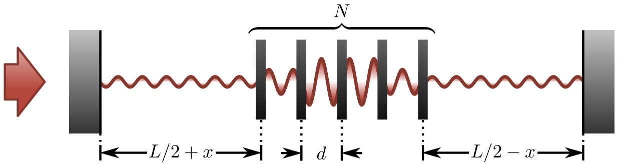

FIG. 3. Schematic of the model we consider. N equidistant elements, each independently harmonically-bound, are positioned in the field of a Fabry–Pérot resonator (we shall consider only the case for which $L \gg Nd$).

A. Element stack inside a cavity

Figure 3 illustrates schematically the periodic element array placed inside a Fabry–Pérot cavity of length L, assumed much longer than the array ($L \gg Nd$). The transfer matrix describing this system is then

$$M_{\mathrm{cav}} \equiv M_{\mathrm{m}}(Z) \cdot M_{\mathrm{p}}(L/2 + x) \cdot M_N \cdot M_{\mathrm{p}}(L/2 - x) \cdot M_{\mathrm{m}}(Z) . \tag{16}$$

Here x is the displacement of the ensemble with respect to its position at the center of the cavity and Z is the polarizability of the cavity mirrors, assumed equal for both. For good, lossless, cavity mirrors ($|Z| \gtrsim 1$), the finesse of the cavity may be simply written $\mathcal{F} = \pi|Z|\sqrt{Z^2+1}$ [64]. The transmission of the system, following Eq. (13), is given by

$$\mathcal{T}_{\mathrm{cav}} = \frac{1}{\left(M_{\mathrm{cav}}\right)_{22}} ; \tag{17}$$

the maxima of $\mathcal{T}_{\mathrm{cav}}$ give the resonances of this system. In order to find these resonances analytically, we consider a simpler system where the cavity mirrors are perfect; we need only solve the relation

$$\begin{pmatrix} 1 \\ -1 \end{pmatrix} \propto \begin{bmatrix} e^{i\theta} & 0 \\ 0 & e^{-i\theta} \end{bmatrix} \times \begin{bmatrix} 1+i\chi & i\chi \\ -i\chi & 1-i\chi \end{bmatrix} \times \begin{bmatrix} e^{i\phi} & 0 \\ 0 & e^{-i\phi} \end{bmatrix} \cdot \begin{pmatrix} 1 \\ -1 \end{pmatrix} , \tag{18}$$

with $\theta \equiv k(L/2 + x) + \mu/2$ and $\phi \equiv k(L/2 - x) + \mu/2$. We thus obtain

$$e^{ikL} = \frac{e^{-i\mu}}{1+i\chi}\left[i\chi\cos(2kx) \pm \sqrt{1+\chi^2\sin^2(2kx)}\right] \tag{19}$$

However, we immediately see that this equation is transcendental in k, and therefore cannot be solved analytically; this equation is easily solvable for L, however, and it therefore easy to solve this equation to find the resonant length of our cavity.

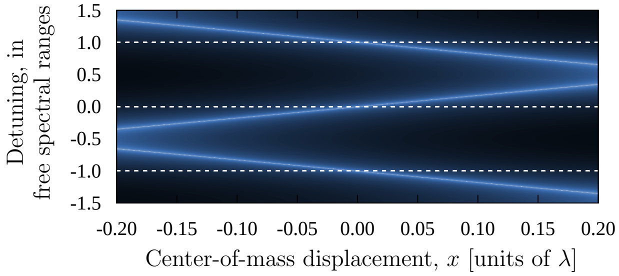

FIG. 4. Transmission through a cavity with $N = 5$ immobile elements configured for maximal reflectivity. The dashed lines denote the bare-cavity resonances, which are shifted due to the presence of the ensemble. x is normalized by a factor $\sqrt{N}$, such that the gradient of the bright curves gives directly the linear optomechanical coupling at that point. ($\zeta = -0.5$, $L \approx 6.3 \times 10^4 \lambda$, $d = d_-$, bare-cavity finesse $\approx 3 \times 10^4$, corresponding to cavity-mirror reflectivities of 99.99%.)

B. Center-of-mass coupling: Reflective optomechanics

It is now a legitimate question to ask: 'If d (or x) shifts by a small amount, how much will the resonant frequency of *this* cavity shift?' This question is, of course, easily answered by expanding Eq. (19) in small increments about its solution. Assuming a dominantly linear effect, we replace $k \to k_0 + \delta k$, $x \to x + \delta x$, $\chi \to \chi + \delta\chi$, and $\mu \to \mu + \delta\mu$ in Eq. (19). Around resonance, the result simplifies to

$$\begin{aligned} L\delta k + \delta\mu = {} & \left[-1 \pm \cos(2k_0x) \middle/ \sqrt{1 + \chi^2 \sin^2(2k_0x)}\right] \\ & \times \delta\chi \big/ \big(1 + \chi^2\big) \\ & \mp \left[2\chi \sin(2k_0x) \middle/ \sqrt{1 + \chi^2 \sin^2(2k_0x)}\right] \\ & \times (x\delta k + k_0\delta x)\,. \end{aligned} \tag{20}$$

We can now use Eq. (20) to compute the coupling strength for the center-of-mass motion of the ensemble. For such a uniform displacement, $\partial\mu = \partial\chi = 0$, and we assume that $|L/x|$ is very large, such that we can write

$$L\delta k = \mp\left[2\chi \sin(2k_0x) \middle/ \sqrt{1 + \chi^2 \sin^2(2k_0x)}\right] k_0\delta x\,. \tag{21}$$

The right-hand-side of this equation is maximized when $\sin(2k_0x) = \mp 1$, whereby

$$L\delta k = 2k_0\big(-\chi/\sqrt{1 + \chi^2}\big)\delta x\,. \tag{22}$$

This is, in absolute value, a monotonically-increasing function of $|\chi|$ and is therefore maximized when χ attains its largest value, $\chi_0 \equiv \zeta\, U_{N-1}\big(\sqrt{1 + \zeta^2}\big) = -i \sin\big[N \cos^{-1}\big(\sqrt{1 + \zeta^2}\big)\big]$. The ensemble attains this reflectivity for when $kd = kd_0 \equiv -\tan^{-1}(\zeta)$ (see Fig. 2). The resulting coupling strength can then be shown to be

$$g_{\mathrm{com}} = g\sqrt{\mathcal{R}/N}\,, \tag{23}$$

where $\mathcal{R} = \chi_0^2/\big(1 + \chi_0^2\big)$. The factor of $1/\sqrt{N}$ that appears in this expression has a natural explanation: The motional mass of N elements is Nm, and therefore the scale of the zero-point-fluctuations is $x_{\mathrm{zpt}}/\sqrt{N}$. We can draw two immediate conclusions regarding g_{com}: (i) $g_{\mathrm{com}} \leq g$, and (ii) g_{com} is optimized for $\mathcal{R} \to 1$. A plot of the transmission spectrum of a cavity with a 5-element ensemble inside it is shown in Fig. 4 as the position of the ensemble is varied. The gradient of the bright curves at each point gives directly the linear optomechanical coupling strength at that point.

The essential aim of this paper is to outline a mechanism [58] whereby coupling strengths much larger than g can be obtained, despite keeping ω_{c} and L fixed. To do this, we shall now explore the coupling strength to the motion of *individual* elements, rather than to the ensemble as a whole.

C. Coupling to each individual element in the transmissive regime

Just as the ensemble attains its peak reflectivity for $d = d_0$, we can see from Fig. 2 that its reflectivity is zero at $d = d_\pm$, where $kd_\pm \equiv -\tan^{-1}(\zeta) \pm \cos^{-1}\big[(1 + \zeta^2)^{-1/2} \cos(\pi/N)\big]$. We now work with this inter-element separation and obtain the optomechanical coupling strength, i.e., the shift in cavity resonance frequency, due to the motion of each element in the ensemble. To allow one element, say the j^{th}, to move independently of the rest of the ensemble, we conceptually split the ensemble into three sections: the elements to the 'left' of j, the j^{th} element itself, and the elements to the 'right' of j. With this logic, the matrix M_N representing the ensemble can be written, for $1 \leq j \leq N$,

$$\begin{aligned} & \begin{bmatrix} e^{i\mu_1/2} & 0 \\ 0 & e^{-i\mu_1/2} \end{bmatrix} \begin{bmatrix} 1 + i\chi_1 & i\chi_1 \\ -i\chi_1 & 1 - i\chi_1 \end{bmatrix} \\ & \quad \times \begin{bmatrix} e^{i(\mu_1/2 + \nu + k\delta x_j)} & 0 \\ 0 & e^{-i(\mu_1/2 + \nu + k\delta x_j)} \end{bmatrix} \\ & \times \begin{bmatrix} 1 + i\zeta & i\zeta \\ -i\zeta & 1 - i\zeta \end{bmatrix} \begin{bmatrix} e^{i(\mu_2/2 + \nu - k\delta x_j)} & 0 \\ 0 & e^{-i(\mu_2/2 + \nu - k\delta x_j)} \end{bmatrix} \\ & \quad \times \begin{bmatrix} 1 + i\chi_2 & i\chi_2 \\ -i\chi_2 & 1 - i\chi_2 \end{bmatrix} \begin{bmatrix} e^{i\mu_2/2} & 0 \\ 0 & e^{-i\mu_2/2} \end{bmatrix}, \end{aligned} \tag{24}$$

where $\nu = kd_\pm$, μ_1 and χ_1 describe the ensemble formed by the $n_1 = j - 1$ membranes to the 'left' of the j^{th}, and μ_2 and χ_2 the one formed by the $n_2 = N - j$ membranes to its 'right'. The displacement of the j^{th} element is denoted δx_j; all other membranes are in their equilibrium position. This small displacement shifts the resonance frequency of the cavity $\omega \to \omega - g_j\delta x_j$, defining g_j as the optomechanical coupling strength for the j^{th} element. In the transmissive regime, to lowest order in $k\delta x_j$ in each entry, the matrix product above can be written, with the

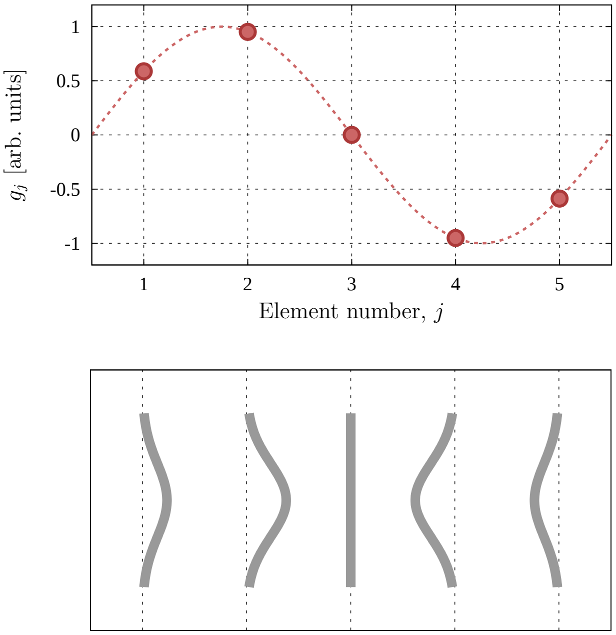

FIG. 5. (Top) Individual coupling strengths for the case of 5 elements; the dashed curve is drawn as a guide to the eye. (Bottom) An illustration of the motional mode that is excited in the ensemble, corresponding to the coupling strengths in the upper figure. We use membranes to make our illustration concrete here, but all our considerations hold for any periodic array of scatterers.

above choice for ν,

$$\begin{bmatrix} e^{i\mu} + \alpha\,\delta x_j & \beta\,\delta x_j \\ \beta^*\,\delta x_j & e^{-i\mu} + \alpha^*\,\delta x_j \end{bmatrix}, \tag{25}$$

where α and β are increments of first order in the relevant displacement [note that the (off-)diagonal terms are complex conjugates of each other; this is different to the case where absorption is nonzero]. When this matrix is substituted into the equation for the resonance condition, the terms involving $\mathrm{Re}\{e^{-i\mu}\alpha\}$ and $\mathrm{Re}\{\beta\}$ drop out entirely *for a symmetric system*, such that it suffices to consider only the imaginary part of the increment. Let us reiterate that this happens only because the off-diagonal terms are complex conjugates of each other; were absorption to be nonzero, this would no longer be the case. Eq. (20) now simplifies to

$$\frac{\partial k}{\partial \delta x_j} = -\frac{\mathrm{Im}\{\beta + e^{-i\mu}\alpha\}}{L + 2d\frac{\partial \chi}{\partial \nu}}, \tag{26}$$

with

$$\alpha = 2ik\zeta\Big[e^{i\mu_1}(1+i\chi_1)\chi_2 - e^{i\mu_2}\chi_1(1+i\chi_2)\Big], \tag{27}$$

and

$$\beta = 2k\zeta\Big[\chi_1\chi_2 - (1+i\chi_1)(1-i\chi_2)e^{i(\mu_1-\mu_2)}\Big], \tag{28}$$

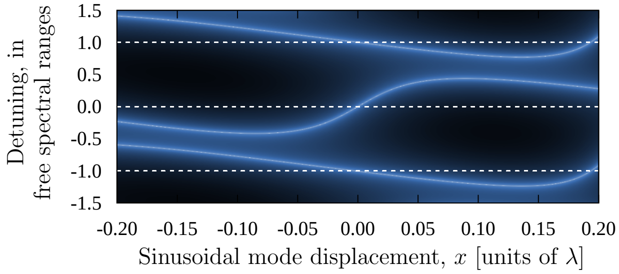

FIG. 6. Transmission through a cavity with $N = 5$ immobile elements in the transmissive regime. This figure should be compared to Fig. 4. x is normalized by a factor $\sqrt{N/2}$. (Parameters as in Fig. 4.)

which we can rewrite, by expressing $\chi_{1,2}$ and $\mu_{1,2}$ in terms of Chebyshev polynomials, as

$$\begin{aligned} \alpha = 2ik\zeta^2\Bigg[&\frac{(1+\zeta^2)U_{n_1-1}^2(a)U_{n_2-1}(a)}{(1-i\zeta)U_{n_1-1}(a) - e^{i\nu}U_{n_1-2}(a)} \\ &- \frac{(1+\zeta^2)U_{n_2-1}^2(a)U_{n_1-1}(a)}{(1-i\zeta)U_{n_2-1}(a) - e^{i\nu}U_{n_2-2}(a)}\Bigg], \end{aligned} \tag{29}$$

and

$$\begin{aligned} \beta = 2k\zeta\Bigg\{&\zeta^2 U_{n_1-1}(a)U_{n_2-1}(a) - \big[1+\zeta^2U_{n_1-1}^2(a)\big] \\ &\times \frac{(1-i\zeta)U_{n_2-1}(a) - e^{i\nu}U_{n_2-2}(a)}{(1-i\zeta)U_{n_1-1}(a) - e^{i\nu}U_{n_1-2}(a)}\Bigg\}. \end{aligned} \tag{30}$$

These two expressions simplify considerably to yield

$$\begin{aligned} \mathrm{Im}\{\beta + e^{-i\mu}\alpha\} &= 2k\zeta\csc\Big(\frac{\pi}{N}\Big) \\ &\times\left[\sqrt{\sin^2\Big(\frac{\pi}{N}\Big)+\zeta^2} - \zeta\right]\sin\left(2\pi\frac{j-\frac{1}{2}}{N}\right), \end{aligned} \tag{31}$$

and therefore, when $\zeta < 0$,

$$\begin{aligned} g_j = -2\omega_c x_0 &\frac{\zeta\csc\big(\frac{\pi}{N}\big)\Big[\sqrt{\sin^2\big(\frac{\pi}{N}\big)+\zeta^2} - \zeta\Big]}{L - 2Nd\zeta\csc^2\big(\frac{\pi}{N}\big)\sqrt{\sin^2\big(\frac{\pi}{N}\big)+\zeta^2}} \\ &\times\sin\left(2\pi\frac{j-\frac{1}{2}}{N}\right). \end{aligned} \tag{32}$$

We illustrate the ‘profile’ of the g_j for $N = 5$ in Fig. 5. As we shall discuss below, the coupling of the collective motion of the membranes to the cavity field is governed by the constant $g_{\sin} \equiv \sqrt{\sum_{j=1}^{N} g_j^2}$, such that for $N = 2$

$$g_{\sin} = -\frac{\sqrt{2}g\,\zeta\big(\sqrt{1+\zeta^2} - \zeta\big)}{1 - 4\frac{d}{L}\zeta\sqrt{1+\zeta^2}}, \tag{33}$$

and for $N > 2$

$$g_{\sin} = -\sqrt{\frac{N}{2}}\,\frac{g\,\zeta\csc\!\left(\frac{\pi}{N}\right)\left[\sqrt{\sin^2\!\left(\frac{\pi}{N}\right)+\zeta^2}-\zeta\right]}{1-2N\frac{d}{L}\zeta\csc^2\!\left(\frac{\pi}{N}\right)\sqrt{\sin^2\!\left(\frac{\pi}{N}\right)+\zeta^2}}\,. \quad (34)$$

This two expressions do not agree upon setting $N = 2$ in the latter; this anomaly is due to the relation

$$\sqrt{\sum_{j=1}^{N}\sin^2\!\left(2\pi\frac{j-\frac{1}{2}}{N}\right)} = \begin{cases}\sqrt{2} & \text{for } N = 2\\ \sqrt{\frac{N}{2}} & \text{for } N > 2\end{cases}. \quad (35)$$

Plots of the type of Fig. 6, similarly to Fig. 4 but now for the case of the sinusoidal mode, can be used to numerically extract $g_{\sin}$, by measuring the gradient of the bright curves. Such data agree with the analytic results derived above.

D. Collective motional-mode treatment: Heisenberg–Langevin formalism

In the preceding section we derived a coupling constant g_j that relates the motion of the j^{th} element to the resonance frequency of the cavity. A particular feature of multi-element arrays is that the cavity field couples to a *collective* motion of the elements, with the g_j playing the role of choosing the 'profile' of the mode that is coupled to the cavity field, in the spirit of Fig. 5. To see this, let us describe the motion of the j^{th} mechanical element ($1 \leq j \leq N$) through the annihilation operator $\hat{b}_j$, which obeys the Heisenberg–Langevin equation of motion [65, 66]

$$\tfrac{\mathrm{d}}{\mathrm{d}t}\hat{b}_j = -(i\omega_{\mathrm{m}}+\Gamma)\hat{b}_j + \hat{F}_j + \sqrt{2\Gamma}\hat{\xi}_j\,, \quad (36)$$

where $\hat{\xi}_j$ is the relevant Langevin noise term whose properties we leave unspecified. For simplicity, we assume that all the oscillators have identical oscillation frequency ω_{m}, decay rate Γ, and temperature T, such that in thermal equilibrium they all have the same average occupation. $\hat{F}_j = g_j\hat{F}$ is a force term due to the action of the cavity, whose exact form is not relevant here. To describe the collective motion, we use the vector $(\tilde{g}_j \equiv g_j/g_{\sin})$, which is naturally normalized such that $\sum_{j=1}^{N}\tilde{g}_j^2 = 1$, and define: $\hat{b} \equiv \sum_{j=1}^{N}\tilde{g}_j\hat{b}_j$ and $\hat{\xi} \equiv \sum_{j=1}^{N}\tilde{g}_j\hat{\xi}_j$. Thus:

$$\tfrac{\mathrm{d}}{\mathrm{d}t}\hat{b} = -(i\omega_{\mathrm{m}}+\Gamma)\hat{b} + g_{\sin}\hat{F} + \sqrt{2\Gamma}\hat{\xi}\,. \quad (37)$$

Under the assumption that the noise terms $\hat{\xi}_j$ are of a similar nature to one another and are independent (i.e., any cross-correlator between $\hat{\xi}_i$ and $\hat{\xi}_j$ is zero for $i \neq j$), then $\hat{\xi}$ obeys the same correlation functions as each *individual* noise term, because of the normalization of $(\tilde{g}_j)$, whereupon $\hat{b}$ behaves as a single collective oscillator with decay rate Γ. Let us remark at this point that our description in terms of this collective mode is one where we merely rotate to a different basis for this N-dimensional space, and therefore the correct normalization, necessary for the rotation to be a unitary operation, is $\sum_{j=1}^{N}\tilde{g}_j^2 = 1$. Therefore, the dynamics of the cavity–mechanical system can be described entirely through an optomechanical Hamiltonian connecting a single cavity mode to a *single collective mechanical mode* with coupling strength $g_{\sin}$, mechanical frequency ω_{m}, decay rate Γ, and noise operator $\hat{\xi}$.

In the next section we investigate some properties of this coupling strength $g_{\sin}$, and draw general conclusions regarding the optomechanical coupling of a transmissive ensemble.

III. TRANSMISSIVE OPTOMECHANICS

Thus far, we have derived an expression for the coupling strength of a cavity field to a periodic array of elements whose compound reflectivity is zero at the cavity frequency. In this section we shall discuss the resulting collective optomechanical coupling. We shall then proceed to discuss one further important consequence of this collective coupling: a linewidth-narrowing effect where the effective linewidth of the cavity resonance decreases over its 'bare' value as the number of elements, or their reflectivity, is increased.

A. Enhanced optomechanical coupling

The first thing we note is the fact that $g_{\sin}$ is no longer bounded above by g. Indeed, for large N and $|\zeta|$ but small d/L, the expression (34) for $g_{\sin}$ simplifies considerably to yield

$$g_{\sin} = \frac{\frac{\sqrt{2}}{\pi}\,g\,\zeta^2N^{3/2}}{1+\frac{2}{\pi^2}\frac{d}{L}\zeta^2N^3} \approx \frac{\sqrt{2}}{\pi}\,g\,\zeta^2N^{3/2}\,. \quad (38)$$

We shall provide numerical examples later to show how $g_{\sin}/g$ can be of the order of 10^2–10^4. To explore the scaling of $g_{\sin}/g$ with N we begin by considering a long cavity ($L \gg d$) and approximate the denominator of Eq. (34) by 1, obtaining

$$g_{\sin} = \sqrt{N/2}\,g|\zeta|\left[\sqrt{1+(N\zeta/\pi)^2}-(N\zeta/\pi)\right], \quad (39)$$

for large N. One can now distinguish between two cases: (i) $(N|\zeta|/\pi) \ll 1$: $g_{\sin}/g = |\zeta|\sqrt{N/2}$, yielding the $\sqrt{N}$-scaling observed in, e.g., atom-cavity optomechanics experiments [67–70] that involve large ensembles of very low reflectivity scatterers. The coupling strength is also multiplied by a factor of $|\zeta|$, which amplifies the interaction when $|\zeta| > 1$; both these features represent a markedly different behavior from the reflective regime. (ii) $(N|\zeta|/\pi) \gg 1$, which gives the $N^{3/2}$- and ζ^2-scaling shown in Eq. (38). This scaling with $N^{3/2}$ is a consequence of the modification of the field mode profile inside the cavity. Indeed, as N increases the fraction of

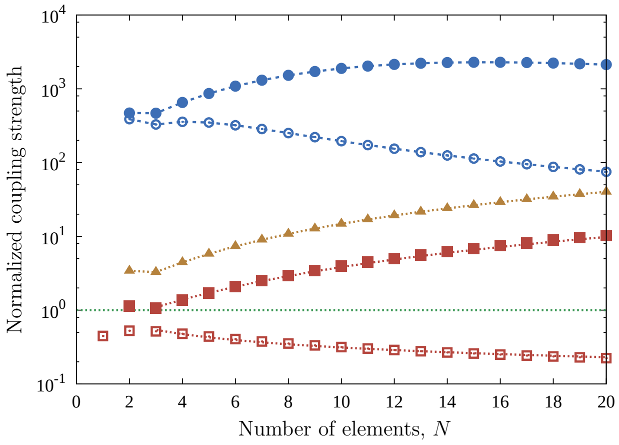

FIG. 7. Collective coupling strength g_{sin} (blue circles, closed red squares, orange triangles) for a cavity of length $L \approx 6.3 \times 10^4\lambda$ and several choices of scatterer reflectivity, compared to the center-of-mass coupling strength g_{com} (open red squares) and g (green line). For the red, orange, and blue data points we choose a per-element intensity reflectivity of 20%, 50%, and 99.4%, respectively. For the center-of-mass data we illustrate the $N^{-1/2}$ scaling law that applies for large N, whereas for the sinusoidal mode we draw a curve through the data points as a guide to the eye. Throughout this plot we take $d = d_-$, except for the data denoted by the open blue circles, for which $d = d_- + 20\lambda$.

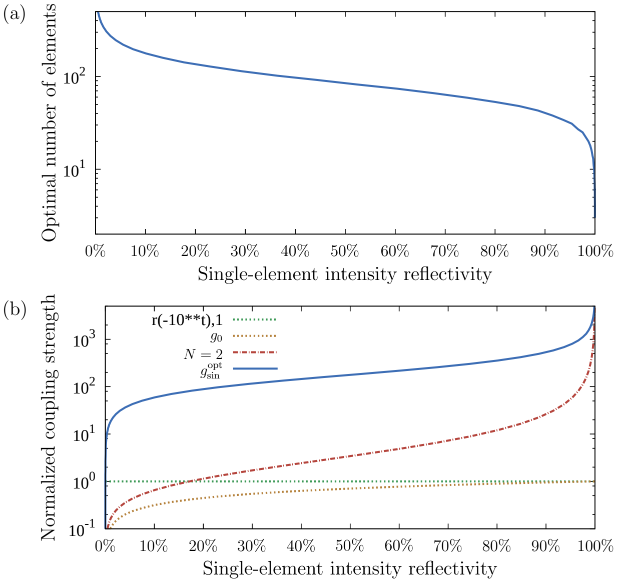

FIG. 8. (a) Optimal number of elements N_{opt}, as a function of the single-element reflectivity. For reflectivities close to 100%, this number decreases rather quickly to $\lesssim 10$. (b) The sinusoidal coupling, normalized to g, optimized as $N = N_{\mathrm{opt}}$ (solid blue curve), compared to the case for $N = 2$ (dashed-dotted red) and g_{com} (dotted orange). For these plots we used $L \approx 6.3 \times 10^4\lambda$ and $d = d_-$.

the energy density per photon inside the array increases strongly; an increased optomechanical coupling strength is consistent with this increase of energy density [71]. The former case, on the other hand, corresponds to an essentially unperturbed cavity field mode, where there is no such concentration of energy density, and a weaker scaling with N is therefore observed.

Similarly, in the behavior of g_{sin}/g as a function ζ for $N = 2$ and in the same 'long cavity' limit, one can distinguish between two regimes [cf. Eq. (33), setting the denominator to 1]. For $|\zeta| \ll 1$, g_{sin}/g grows linearly with $|\zeta|$ as a consequence of the increased reflectivity of each element. For $|\zeta| \gg 1$, however, the cavity field mode is modified substantially and is strongly concentrated in the region between the two elements. This concentration grows quickly as a function of $|\zeta|$ and gives rise to a quadratic scaling of g_{sin}/g with $|\zeta|$.

The denominator in the full form of Eq. (38) can be interpreted as an effective renormalization of the cavity length from L to $L_{\mathrm{eff}} \equiv L + \frac{2}{\pi^2} d\zeta^2 N^3$. We shall discuss the regime in which the effective length is significantly larger than L, where an interesting linewidth-narrowing effect occurs, in greater detail in Sec. III B below. We have already seen that for N, $|\zeta|$, and d/L small enough that $L_{\mathrm{eff}} \approx L$ the coupling strength scales as $\zeta^2 N^{3/2}$. On the other hand, when the parameters are such that $L_{\mathrm{eff}} \gg L$, g_{sin} does not depend on ζ and decreases as $N^{-3/2}$. We say that, in transitioning between the two scaling laws, g_{sin} *saturates* (i.e., reaches a maximum value at some finite value for N) before it starts decreasing.

Optimizing g_{sin} over N for arbitrary L/d, in this manner, we obtain $g_{\mathrm{sin}}^{\mathrm{opt}} = \frac{1}{2} g\sqrt{L/d}|\zeta|$. This expression is valid for $|\zeta|$ that is not too large, since the optimal number of elements must be ≥ 2. This favorable scaling with both N and $|\zeta|$ is a significant improvement over the state of the art. Close inspection reveals that $g_{\mathrm{sin}}^{\mathrm{opt}}$ is proportional to $1/\sqrt{Ld}$ and therefore can be improved either by making the main cavity smaller (i.e., decreasing L) or, independently, by positioning the elements closer together (decreasing d to a smaller value whilst maintaining the condition of zero reflectivity).

Alternatively, one may optimize the parameters such that the second term in the denominator of Eq. (38) dominates, i.e., where $L_{\mathrm{eff}} \gg L$. The coupling strength then takes the approximate form

$$\frac{\pi}{\sqrt{2}} g \frac{L}{d} N^{-3/2} \xrightarrow[N=2]{} \frac{\pi}{2} g_{\mathrm{sm}}\,, \tag{40}$$

where we have taken the optimal ($N = 2$) case and defined $g_{\mathrm{sm}} \equiv \omega_{\mathrm{c}} x_{\mathrm{zpt}}/d$ as the optomechanical coupling strength for a (small) cavity of length d with a single moving mirror. In this regime, therefore, the system acts as a small cavity of length d and is sensitive to relative motion between the two elements but not to the length of the main cavity. Figure 7 illustrates, primarily, the enhancement of optomechanical coupling strength that can be obtained by operating in the transmissive regime as compared to coupling to the center-of-mass motion. Several important observations can be made from this figure. The largest value for g_{sin} increases with $|\zeta|$; in the figure we show data points for $\zeta = -0.5$ (20% intensity reflectivity; red data), $\zeta = -0.5$ (50%; orange) and $\zeta = -12.9$ (99.4%; blue), the first two of which represents a typical reflectivity for SiN membranes used for optomechanical experiments [72], and the last membranes with increased reflectivity due to the use of sub-wavelength patterning [73, 74]. Secondly, the value of N for which the coupling strength is optimized is highly dependent on the value of d; the reflectivity of the array depends on $d \mod (\lambda/2)$, so that one is free to increase the element spacing by integer multiples of half a wavelength without affecting its transmission properties (in the limit of a wavelength-independent reflectivity). However, the coupling strength is sensitive to this increase: The larger d/L is, the earlier the *saturation point* is reached, beyond which increasing N lowers the coupling strength. The figure also illustrates two scaling laws that we derived above. The center-of-mass coupling decreases, for $N \gtrsim 3$, as $N^{-1/2}$, whereas the sinusoidal coupling strength g_{sin} scales approximately as $N^{3/2}$ for N large enough, but also small enough to avoid the effects of saturation. These two scaling laws are illustrated by the red dotted curves, drawn as guides to the eye. By contrast, the other curves and all the data points are generated using the full analytical formulae, which are in excellent agreement with numeric calculations.

In Fig. 8 we study (a) the optimal number of elements required, N_{opt}, and (b) the resulting coupling, as a function of the polarizability of each element in the array. For weakly reflective elements, as illustrated in Fig. 8(a), the coupling only saturates for very large values of N, whereas as the reflectivity of the elements increases the optimal number of elements decreases, at first steadily and then quite sharply, until it reaches a point where the coupling strength decreases for $N > 2$. This curve is sensitive to the ratio d/L; smaller values of this ratio result in larger values for N_{opt}. In panel (b), we illustrate the optimized sinusoidal coupling strength (solid blue curve), as well as the coupling strength for $N = 2$ (dashed-dotted red) and the center-of-mass coupling (dotted orange). Two immediate observations can be made that are quite general. First, g_{sin} may exceed g_{com} by several orders of magnitude. Second, in the case of weakly-reflective elements, it is necessary to use rather large values for N to achieve this orders-of-magnitude improvement in coupling strength.

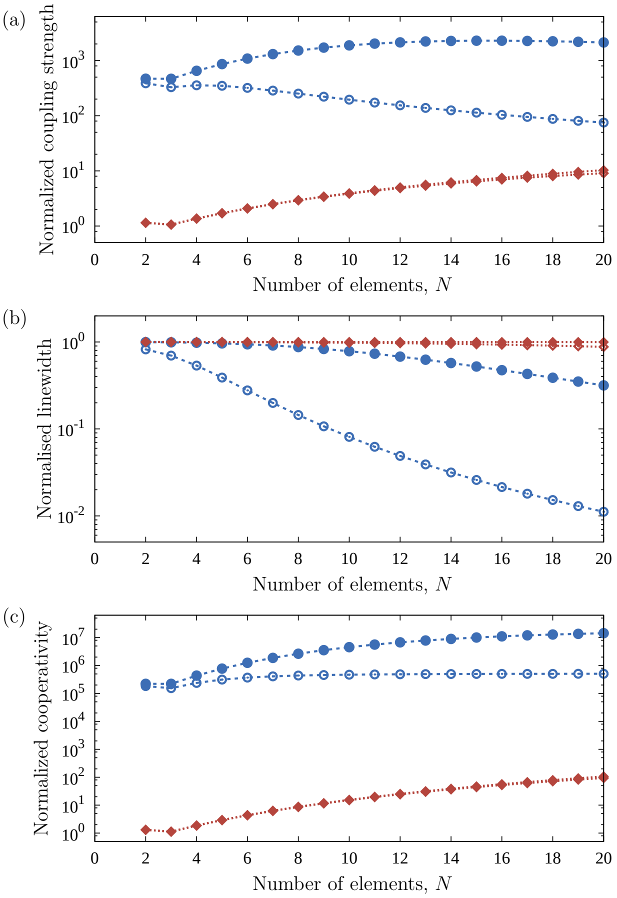

FIG. 9. (a) Coupling strength, normalized to g, as a function of the number of elements. Four sets of data are shown. The red diamonds (blue circles) correspond to a single-element reflectivity of 20% (99.4%). Closed (open) symbols represent an inter-element spacing of $d = d_-$ ($d = d_- + 20\lambda$). We note that the inter-element separation has a much stronger effect for highly-reflective elements. ($L \approx 6.3 \times 10^4 \lambda$, bare-cavity finesse $\approx 3 \times 10^4$.) (b) A similar plot showing the effective cavity linewidth, normalized to the bare-cavity linewidth, obtained in each of the cases displayed in the upper plot. (c) Putting these two together we can calculate the cooperativity, normalized to the single-element cooperativity, and demonstrate an enhancement by several orders of magnitude for the chosen parameters.

B. Linewidth narrowing

The saturation phenomenon described above reveals another interesting effect as the number of elements is increased beyond N_{opt}: The presence of the array inside the cavity acts to narrow the cavity linewidth. The physical basis behind this is rather transparent and relies on two observations. First, the fact that the array is transparent at the cavity resonance frequency means that the finesse of the cavity – which is related to the number of round-trips a photon makes inside the cavity on average – *is unchanged* by its presence. The second observation is that, as we have already noted, Eq. (38) reveals that the cavity is effectively lengthened to a length L_{eff}. Since the bare-cavity linewidth is $\kappa_{\text{c}} \propto 1/(\mathcal{F}L)$, it follows that the linewidth of the cavity is reduced to $\kappa_{\text{eff}} \propto 1/(\mathcal{F}L_{\text{eff}})$. By choosing the right parameters, one can optimize for this linewidth-narrowing effect, Fig. 9(b), to narrow the optical resonance substantially. As several mechanisms in optomechanics, e.g., cooling in the linearized regime, are improved in the so-called 'resolved sideband' regime, where $\omega_{\text{m}} \gg \kappa_{\text{c}}$, the collective mechanism we describe can result in the condition $\kappa_{\text{c}} > \omega_{\text{m}} \gg \kappa_{\text{eff}}$ being satis-

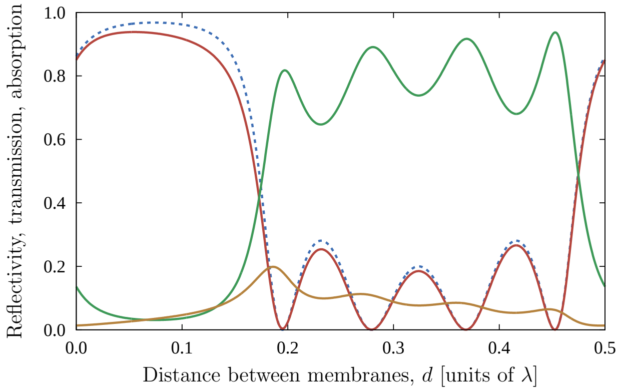

FIG. 10. Reflectivity (red), transmission (green), and absorption (orange) for $N = 5$ elements with an individual reflectivity of ca. 50% and an absorption of ca. 1.6% per element. The dashed blue curve is identical to the solid blue curve in Fig. 2. Note that the absorption around the transmissive points is highest close to d_+ and lowest close to d_-.

fied, thereby improving the performance of these mechanisms in the system.

One other figure-of-merit that is relevant to several mechanisms is the cooperativity $C = g^2/(\kappa\Gamma)$, i.e., the ratio of the square of the optomechanical coupling strength to the product of the optical and mechanical decay rates, κ and Γ, respectively. For a multi-element system composed of independent oscillators and operating in the transmissive regime, Γ is independent of N, but $g_{\mathrm{sin}} \sim N^{3/2}$ and $\kappa_{\mathrm{c}} \sim N^3$ in the appropriate regime; this is illustrated in Fig. 9(a) and (b). The result is a competition between these two factors, yielding a constant cooperativity as N is increased. In Fig. 9(c) we plot the *normalized* cooperativity, i.e., the cooperativity for the N-element ensemble divided by that for a single element; the enhancement obtained with the parameters used is of almost 10^6. Even when absorption is included, as explained below in Sec. IV A, an enhancement of several orders of magnitude is still possible [58].

IV. RESILIENCE TO ABSORPTION AND IMPERFECTIONS

In this section we address questions regarding the resilience of the mechanism we introduce in the face of experimental imperfections in the positioning, reflectivity, and absorption of individual elements.

A. Effects of absorption in the elements

For a nonzero per-element absorption, the largest amount of absorption appears close to the points where the ensemble is transparent. This is shown in Fig. 10, where we plot the reflectivity, transmission, and absorption of an ensemble of 5 elements as the spacing between the elements is scanned; this figure is meant to complement Fig. 2. A general feature is that the absorption is largest at d_+ and rather smaller at d_-; we have therefore chosen the latter as our working point throughout this paper.

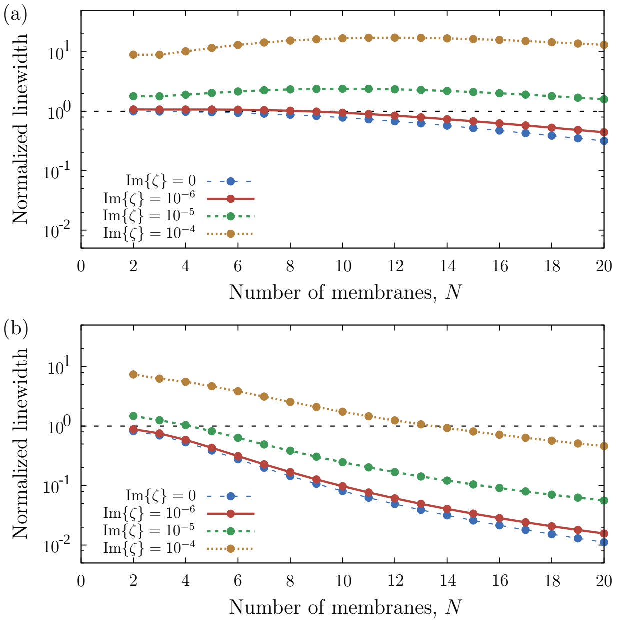

FIG. 11. Effect of increasing absorption on the linewidth (normalized to the bare-cavity linewidth) for a single-element reflectivity of 99.4% and (a) $d = d_-$, (b) $d = d_- + 20\lambda$. Larger inter-element separations make the system more tolerant to higher levels of absorption. The linewidth of the bare cavity is represented by the horizontal dashed black lines. These figures should be compared to the data shown in solid blue circles Fig. 9(b). (Bare-cavity finesse $\approx 3 \times 10^4$, other parameters as in Fig. 9.)

A systematic study of the effect of absorption on the cavity linewidth is shown in Fig. 11. The cavity linewidth, both in the presence of absorption and in its absence, is calculated numerically by scanning over, and fitting a Lorentzian to, the cavity resonance. An approximate expression for the linewidth in the presence of absorption can be given by taking into account the optical losses in the ensemble through a nonzero $\mathrm{Im}\{\zeta\}$, yielding

$$\kappa_{\mathrm{eff,abs}} = \frac{c}{2\left(L + \frac{2}{\pi^2} d|\zeta|^2 N^3\right)} \left(\frac{1}{|Z|\sqrt{Z^2+1}} + 2A \right) \quad (41)$$

$$= \kappa_{\mathrm{eff}} \left(1 + 2A|Z|\sqrt{Z^2+1}\right), \quad (42)$$

where the factor A corresponds to the single-pass absorption for the ensemble, and κ_{eff} is evaluated with $\zeta \to -|\zeta|$. For $d = d_-$, $\mathrm{Im}\{\zeta\} \lll 1$, and $N \geq 2$, A is given approx-

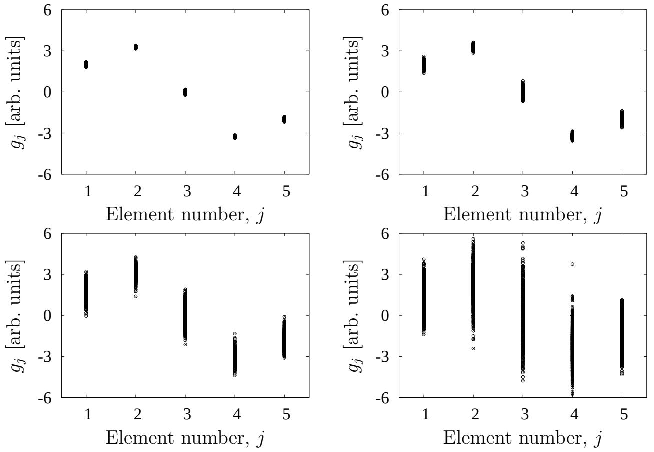

FIG. 12. Profiles of the 'sinusoidal mode' (i.e., the coupling strength of each element, in arbitrary units) in a 5-element array, for a representative sample of 1000 populations, for a total of 4000 populations, demonstrating random positioning errors of varying degree. The position of each element is varied from the ideal case by a random number drawn from a Gaussian distribution with standard deviation, from left to right, of $10^{-3}\lambda$, $10^{-2.5}\lambda$, $10^{-2}\lambda$, and $10^{-1.5}\lambda$. The overall coupling strength resulting from each of these simulations is shown in Fig. 13. ($\zeta = -0.5$, $d = d_-$, other parameters as in Fig. 9.)

imately by

$$2\,\mathrm{Im}\{\zeta\}\sin(\nu)\big[\zeta\cos(\nu)+\sin(\nu)\big]U'_{N-1}\big[\cos(\pi/N)\big] \approx \frac{2N\,\mathrm{Im}\{\zeta\}}{1-\cos\left(\frac{2\pi}{N}\right)}\left(\sqrt{1+|\zeta|^2}\sin\left\{2\left[\arccos\left(\frac{\cos\left(\frac{\pi}{N}\right)}{\sqrt{1+|\zeta|^2}}\right)-\arctan(|\zeta|)\right]-\mathrm{arccot}(|\zeta|)\right\}+1\right), \tag{43}$$

where $\nu = kd_-$ and $U'_n(x)$ is the first derivative of the n^{th} Chebyshev polynomial with respect to its argument. Upon substituting this expression for A, $\kappa_{\mathrm{eff,abs}}$ agrees with the numerically-calculated data shown in Fig. 11. For large N and $|\zeta|$ (but $\mathrm{Im}\{\zeta\} \lll 1$) we find $A \approx N\,\mathrm{Im}\{\zeta\}$.

To stay within the frame of the 1D model considered here, a small misalignment in the individual elements can be modeled similarly to absorption, since both effects represent a loss channel for the cavity field. Other detrimental effects of absorption, such as heating, are mitigated by the large coupling strengths obtained, which allow much smaller photon numbers to be used ($g_{\mathrm{sin}}^2 \propto N^3$ increases faster than the absorbed power as N increases). We note also that at large input powers it might be possible to exploit photothermal forces to further enhance, or change the nature of, the collective optomechanical interaction [75–79].

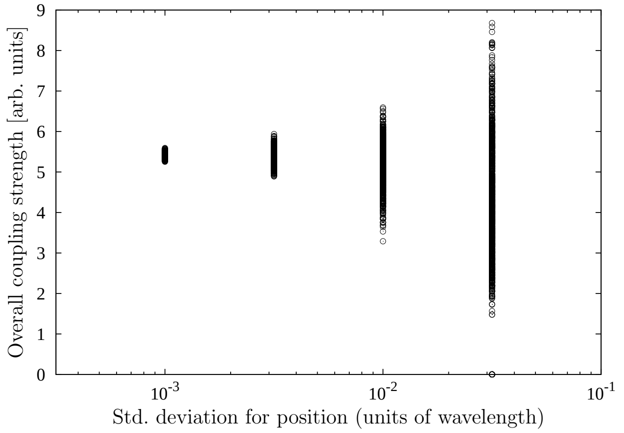

FIG. 13. Overall coupling strength for the populations shown in Fig. 12. Compared to the ideal case, the coupling strength for the four cases has an average (standard deviation) of 0.0% (1.0%), −0.3% (3.0%), −3.4% (9.4%), and −21.5% (37.2%). (Parameters as in Fig. 12.)

B. Inhomogeneities in the system

Here we discuss the behavior of the system in the face of two experimentally realistic sources of inhomogeneity: positioning errors and imperfections leading to different absorption in the elements making up the array. To address the issue of positioning errors, we performed numerical simulations with several thousand arrays ($N = 5$, $\zeta = -0.5$, $L \approx 6.3 \times 10^4\lambda$, $d = d_-$) whose elements were each shifted from the optimal position by a random shift drawn from a Gaussian distribution with a standard deviation of 10 nm. The resulting coupling strengths were within ±10% of the analytically-calculated value. A representative sample of the analysis, extended to broader Gaussian distributions and performed on 4000 arrays, is shown in Fig. 12 and Fig. 13.

Until now, for the most part, the elements making up the array were assumed to be identical and non-absorbing; the latter is an excellent approximation to a single membrane with an imaginary part of the refractive index being $\lesssim 10^{-6}$–10^{-5} [80, 81]. Fluctuations in the polarizability of the individual elements by up to ±10% give coupling strengths within ±6% of the analytic value. Our numerical investigations show that the major effect of absorption is not on the optomechanical coupling strength, but on the linewidth of the cavity. High levels of absorption would therefore not alter the coupling strength significantly, but would limit the achievable cavity finesse.

V. NUMERICAL EXAMPLES

In this section we give two numerical examples, one using readily-available membranes and the other state-of-the-art highly-reflective ones, to demonstrate the power of transmissive optomechanics. If we take commercial silicon nitride membranes [72, 80, 82, 83] with an intensity reflectivity of 20% ($\zeta = -0.5$) and $x_0 = 1.8\,\mathrm{fm}$, and a cavity with $L = 6.7\,\mathrm{cm}$ and a wavelength of 1064 nm, we can estimate $g_{\mathrm{com}} \approx 2\pi \times (12.8 \times N^{-1/2}\,\mathrm{Hz})$ for $N \gtrsim 3$. For the sinusoidal mode, and with the same parameters, $g_{\mathrm{sin}} \approx 2\pi \times (1.3 \times N^{3/2}\,\mathrm{Hz})$ for large N; an improvement by over an order of magnitude when $N = 10$ (cf. Fig. 7). Suppose, now, that we consider instead highly-reflective membranes [73, 74] having 99.4% intensity reflectivity ($\zeta = -12.9$), $x_0 = 2.7\,\mathrm{fm}$, and $\omega_{\mathrm{m}} = 2\pi \times 211\,\mathrm{kHz}$. For a 0.25 cm-long cavity with finesse $F = 1.2 \times 10^5$, $d = d_-$, and $N = 5$ membranes, one obtains $g_{\mathrm{com}} \approx 2\pi \times 600\,\mathrm{Hz}$ and $g_{\mathrm{sin}} \approx 2\pi \times 270\,\mathrm{kHz}$, which is larger than both ω_{m} and $\kappa_{\mathrm{c}} = 2\pi \times 250\,\mathrm{kHz}$. At a temperature of 1 K and with a mechanical quality factor of 10^6 the *single-photon* cooperativity is ca. 14 for this system; strong coupling between a single photon and a single phonon is already within reach with only a few elements.

Moving away from highly-reflective scatterers, we can apply our results to systems of very low reflectivity, such as atoms, molecules, dielectric microspheres, etc. It should be first noted that all these systems have a reflectivity on the order of 10^{-6}, which means that $N|\zeta| \ll 1$ in typical experiments (for example with cold atoms in cavities [67–70]), i.e., the particles do not significantly modify the mode structure of the cavity resonance. In this case g_{sin} reduces to the expected $N^{1/2}$ scaling that arises from the independent coupling of well-localized scatterers interacting with an unmodified cavity field [67–70]. We note, however, that recent experiments [84] using "pancake"-shaped clouds of cold atoms in an optical lattice have shown intensity reflectivities as high as 80% and are approaching a regime where the effects discussed previously may be observed.

VI. CONCLUDING REMARKS

Transmissive optomechanics presents a departure from traditional optomechanical systems in that the reflectivity of a compound element is purposely engineered to be as close to zero as possible. A wealth of interesting effects exist in this regime, not least (i) the possibility of strongly increasing the optomechanical cooperativity and obtaining strong coupling between a single photon and a single phonon, (ii) the existence of a linewidth-narrowing mechanism that renders the resolved-sideband regime of optomechanics more accessible, (iii) the existence of long-range interactions within optomechanical arrays [58], and (iv) the possibility to enhance optomechanical nonlinearities [40]. The system we described may be composed of any periodic array of linearly-interacting polarizable scatterers, e.g, an ensemble of macroscopic dielectric scatterers, or even atoms in an optical lattice, and therefore presents a widely-configurable and robust basis for investigating strong and collective effects in optomechanical or electromechanical setups.

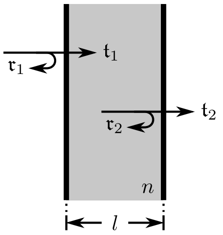

FIG. 14. Modeling an individual membrane as a plate of thickness l and refractive index n.

ACKNOWLEDGEMENTS

We acknowledge support from the Royal Commission for the Exhibition of 1851 (A.X.), Austrian Science Fund (FWF): P24968-N27 and an STSM grant from the COST Action MP1006 "Fundamental problems in quantum physics" (C.G.), and the EU CCQED and PICC projects, and Danish Council for Independent Research under the Sapere Aude program (A.D.). We would also like to thank J. Bateman, K. Hammerer, I. D. Leroux, M. Paternostro, and H. Ritsch for fruitful discussions.

Appendix A: Polarizability of thin dielectric plates

We model each membrane, or any other thin dielectric scatterer, as a plate of (real) refractive index n and thickness l (see Fig. 14). Going from left to right, the two interfaces have amplitude reflectivities $\mathfrak{r}_1 = \mathfrak{r} = (1-n)/(1+n)$ and $\mathfrak{r}_2 = -\mathfrak{r}$, as well as transmissivities $\mathfrak{t}_1 = 2/(1+n)$ and $\mathfrak{t}_2 = 2n/(1+n)$, which are obtained from the respective Fresnel coefficients at normal incidence. The amplitude reflection and transmission coefficients for light of wavenumber $k = \omega/c$ incident on the plate as a whole can then be written

$$r = \frac{\mathfrak{r}\big(1 - e^{-2inkl}\big)}{1 - \mathfrak{r}^2 e^{-2inkl}}\,, \text{ and } t = \frac{\mathfrak{t}_1\mathfrak{t}_2 e^{-inkl}}{1 - \mathfrak{r}^2 e^{-2inkl}}\,, \tag{A1}$$

respectively. We then define the effective membrane polarizability $\zeta \equiv -ir/t$ [59], whereupon

$$\zeta = \frac{2\mathfrak{r}}{\mathfrak{t}_1\mathfrak{t}_2}\sin(nkl) = \frac{1-n^2}{2n}\sin(nkl)\,. \tag{A2}$$

The 'thin membrane' approximation corresponds to taking $n \gg 1$ but $nkl \ll 1$, whereby we may approximate

$$\zeta = -\tfrac{1}{2}n^2 kl\,. \tag{A3}$$

This justifies our assertion throughout this paper that $\zeta < 0$ for lossless scatterers. Let us now calculate the relative change in ζ over a frequency interval of size $\delta\omega = c\delta k$ centred around the frequency ω:

$$\frac{\partial\zeta/\partial k}{\zeta}\delta k = \frac{nkl}{\tan(nkl)}\frac{\delta\omega}{\omega}\,. \tag{A4}$$

Throughout the main text, we were interested in the optomechanical behavior of arrays of such structures inside cavities. We may then reasonably take $\delta\omega/\omega = 1/Q$, where the quality factor Q of an optical cavity is generally of the order of 10^7–10^9. Under the thin membrane approximation one can write

$$\frac{\partial\zeta/\partial k}{\zeta}\delta k = \frac{1}{Q}\,. \qquad \text{(A5)}$$

For membranes that are thin on the scale of a wavelength, this requirement is thus satisfied trivially; for thicker membranes one must take care to avoid the structural resonances at $\sin(nkl) = 0$. Another reason for requiring the membranes to be thin is that the free-spectral range of each 'membrane-etalon' must be significantly larger than that of the main cavity, which requires $l \lll L/n$, where L is the length of the cavity. A final, and stronger, requirement is that the entire membrane stack should fit within the Rayleigh range of the cavity mode.

Appendix B: Polarizability of two-level atoms

For a single two-level atom (TLA) at the waist of a Gaussian field of mode area σ_{L}, we may write

$$\zeta = -\frac{\sigma_{\mathrm{a}}}{2\sigma_{\mathrm{L}}}\frac{\gamma}{i\Delta+\gamma}\,, \qquad \text{(B1)}$$

where γ is the (half-width at half-maximum) linewidth of the atomic resonance and $\Delta = \omega_{\mathrm{L}} - \omega_{\mathrm{a}}$ the detuning between the driving field (frequency ω_{L}) and atomic resonance (ω_{a}). $\sigma_{\mathrm{a}} = 3\lambda_{\mathrm{a}}^2/(2\pi)$ is the resonant radiative cross-section of the atom at a wavelength $\lambda_{\mathrm{a}} = 2\pi c/\omega_{\mathrm{a}}$. A first-principles derivation of this relation can be found in Ref. [64]. A 'non-absorbing' scatterer, where ζ is real, can be approximated by a TLA when $|\Delta| \gg \gamma$.
The expression above assumes that one is working in the regime of low saturation, where the excited state population is negligible. Under these conditions, the effect of having m atoms inside the waist of the Gaussian beam is simply $\zeta \to m\zeta$.

---

[1] M. Aspelmeyer, T. J. Kippenberg, and F. Marquardt, e-print (2013), arXiv:1303.0733.

[2] P. Meystre, Ann. Phys. **525**, 215 (2013).

[3] J. D. Teufel, T. Donner, D. Li, J. W. Harlow, M. S. Allman, K. Cicak, A. J. Sirois, J. D. Whittaker, K. W. Lehnert, and R. W. Simmonds, Nature **475**, 359 (2011).

[4] J. Chan, T. P. M. Alegre, A. H. Safavi-Naeini, J. T. Hill, A. Krause, S. Gröblacher, M. Aspelmeyer, and O. Painter, Nature **478**, 89 (2011).

[5] E. Verhagen, S. Deléglise, S. Weis, A. Schliesser, and T. J. Kippenberg, Nature **482**, 63 (2012).

[6] A. H. Safavi-Naeini, J. Chan, J. T. Hill, T. P. M. Alegre, A. Krause, and O. Painter, Phys. Rev. Lett. **108**, 033602 (2012).

[7] N. Brahms, T. Botter, S. Schreppler, D. W. C. Brooks, and D. M. Stamper-Kurn, Phys. Rev. Lett. **108**, 133601 (2012).

[8] D. W. C. Brooks, T. Botter, S. Schreppler, T. P. Purdy, N. Brahms, and D. M. Stamper-Kurn, Nature **488**, 476 (2012).

[9] A. H. Safavi-Naeini, S. Groeblacher, J. T. Hill, J. Chan, M. Aspelmeyer, and O. Painter, e-print (2013), arXiv:1302.6179.

[10] T. P. Purdy, R. W. Peterson, and C. A. Regal, Science **339**, 801 (2013).

[11] M. Eichenfield, J. Chan, R. M. Camacho, K. J. Vahala, and O. Painter, Nature **462**, 78 (2009).

[12] S. Gröblacher, K. Hammerer, M. R. Vanner, and M. Aspelmeyer, Nature **460**, 724 (2009).

[13] K. Borkje, A. Nunnenkamp, J. D. Teufel, and S. M. Girvin, e-print (2013), arXiv:1304.4155.

[14] M.-A. Lemonde, N. Didier, and A. A. Clerk, e-print (2013), arXiv:1304.4197.

[15] U. Akram, N. Kiesel, M. Aspelmeyer, and G. J. Milburn, New J. Phys. **12**, 083030 (2010).

[16] P. Rabl, Phys. Rev. Lett. **107**, 063601 (2011).

[17] A. Nunnenkamp, K. Børkje, and S. M. Girvin, Phys. Rev. Lett. **107**, 063602 (2011).

[18] A. Nunnenkamp, K. Børkje, and S. M. Girvin, Phys. Rev. A **85**, 051803 (2012).

[19] J. Qian, A. A. Clerk, K. Hammerer, and F. Marquardt, Phys. Rev. Lett. **109**, 253601 (2012).

[20] M. Ludwig, A. H. Safavi-Naeini, O. Painter, and F. Marquardt, Phys. Rev. Lett. **109**, 063601 (2012).

[21] K. Stannigel, P. Komar, S. J. M. Habraken, S. D. Bennett, M. D. Lukin, P. Zoller, and P. Rabl, Phys. Rev. Lett. **109**, 013603 (2012).

[22] A. Kronwald, M. Ludwig, and F. Marquardt, Phys. Rev. A **87**, 013847 (2013).

[23] J.-Q. Liao and C. K. Law, Phys. Rev. A **87**, 043809 (2013).

[24] S. Mancini, V. Giovannetti, D. Vitali, and P. Tombesi, Phys. Rev. Lett. **88**, 120401 (2002).

[25] J. Zhang, K. Peng, and S. L. Braunstein, Phys. Rev. A **68**, 013808 (2003).

[26] W. Marshall, C. Simon, R. Penrose, and D. Bouwmeester, Phys. Rev. Lett. **91**, 130401 (2003).

[27] J. Eisert, M. B. Plenio, S. Bose, and J. Hartley, Phys. Rev. Lett. **93**, 190402 (2004).

[28] M. Pinard, A. Dantan, D. Vitali, O. Arcizet, T. Briant, and A. Heidmann, Europhys. Lett. **72**, 747 (2005).

[29] D. Vitali, S. Mancini, and P. Tombesi, J. Phys. A: Math. Theor. **40**, 8055 (2007).

[30] C. Genes, D. Vitali, and P. Tombesi, New J. Phys. **10**, 095009 (2008).

[31] M. Bhattacharya, H. Uys, and P. Meystre, Phys. Rev. A **77**, 033819 (2008).

[32] M. Bhattacharya and P. Meystre, Phys. Rev. A **78**, 041801 (2008).

[33] M. J. Hartmann and M. B. Plenio, Phys. Rev. Lett. **101**, 200503 (2008).

[34] M. Ludwig, K. Hammerer, and F. Marquardt, Phys. Rev. A **82**, 012333 (2010).

[35] H. Miao, S. Danilishin, T. Corbitt, and Y. Chen, Phys. Rev. Lett. **103**, 100402 (2009).

[36] J. M. Dobrindt and T. J. Kippenberg, Phys. Rev. Lett. **104**, 033901 (2010).

[37] X. Xu and J. M. Taylor, e-print (2013), arXiv:1303.7469.

[38] H. Seok, L. F. Buchmann, S. Singh, and P. Meystre, Phys. Rev. A **86**, 063829 (2012).

[39] P. Kómár, S. D. Bennett, K. Stannigel, S. J. M. Habraken, P. Rabl, P. Zoller, and M. D. Lukin, Phys. Rev. A **87**, 013839 (2013).

[40] C. Genes, A. Xuereb, G. Pupillo, and A. Dantan, e-print (2013), arXiv:1304.1715.

[41] K. Stannigel, P. Rabl, A. S. Sørensen, P. Zoller, and M. D. Lukin, Phys. Rev. Lett. **105**, 220501 (2010).

[42] D. E. Chang, A. H. Safavi-Naeini, M. Hafezi, and O. Painter, New J. Phys. **13**, 023003 (2011).

[43] K. Jacobs, e-print (2012), arXiv:1209.2499.

[44] S. Rips, M. Kiffner, I. Wilson-Rae, and M. J. Hartmann, New J. Phys. **14**, 023042 (2012).

[45] G. Heinrich, J. G. E. Harris, and F. Marquardt, Phys. Rev. A **81**, 011801 (2010).

[46] G. Heinrich, M. Ludwig, J. Qian, B. Kubala, and F. Marquardt, Phys. Rev. Lett. **107**, 043603 (2011).

[47] D. Marcos, A. Tomadin, S. Diehl, and P. Rabl, New J. Phys. **14**, 055005 (2012).

[48] U. Akram, W. Munro, K. Nemoto, and G. J. Milburn, Phys. Rev. A **86**, 042306 (2012).

[49] M. Ludwig and F. Marquardt, e-print (2012), arXiv:1208.0327.

[50] I. S. Grudinin, H. Lee, O. Painter, and K. J. Vahala, Phys. Rev. Lett. **104**, 083901 (2010).

[51] Q. Lin, J. Rosenberg, D. Chang, R. Camacho, M. Eichenfield, K. J. Vahala, and O. Painter, Nat. Photonics **4**, 236 (2010).

[52] I. Mahboob, E. Flurin, K. Nishiguchi, A. Fujiwara, and H. Yamaguchi, Nat. Commun. **2**, 198 (2011).

[53] I. Mahboob, K. Nishiguchi, H. Okamoto, and H. Yamaguchi, Nat. Phys. **8**, 387 (2012).

[54] F. Massel, T. T. Heikkila, J.-M. J.-M. Pirkkalainen, S. U. Cho, H. Saloniemi, P. J. Hakonen, M. A. Sillanpaa, T. T. Heikkilä, and M. A. Sillanpää, Nature **480**, 351 (2011).

[55] K. Zhang, P. Meystre, and W. Zhang, Phys. Rev. Lett. **108**, 240405 (2012).

[56] T. Botter, D. W. C. Brooks, S. Schreppler, N. Brahms, and D. M. Stamper-Kurn, Phys. Rev. Lett. **110**, 153001 (2013).

[57] D. M. Stamper-Kurn, e-print (2012), arXiv:1204.4351.

[58] A. Xuereb, C. Genes, and A. Dantan, Phys. Rev. Lett. **109**, 223601 (2012).

[59] I. H. Deutsch, R. J. C. Spreeuw, S. L. Rolston, and W. D. Phillips, Phys. Rev. A **52**, 1394 (1995).

[60] A. Xuereb, P. Domokos, J. Asbóth, P. Horak, and T. Freegarde, Phys. Rev. A **79**, 053810 (2009).

[61] N. Miladinovic, F. Hasan, N. Chisholm, I. E. Linnington, E. A. Hinds, and D. H. J. O'Dell, Phys. Rev. A **84**, 043822 (2011).

[62] P. Yeh, *Optical Waves in Layered Media*, 2nd ed. (Wiley, Hoboken, New Jersey, 2005).

[63] A. Xuereb and P. Domokos, New J. Phys. **14**, 095027 (2012).

[64] A. Xuereb, *Optical Cooling Using the Dipole Force*, Springer Theses (Springer, Heidelberg, 2012).

[65] V. Giovannetti and D. Vitali, Phys. Rev. A **63**, 023812 (2001).

[66] C. Genes, D. Vitali, P. Tombesi, S. Gigan, and M. Aspelmeyer, Phys. Rev. A **77**, 033804 (2008).

[67] D. Kruse, M. Ruder, J. Benhelm, C. von Cube, C. Zimmermann, P. W. Courteille, T. Elsässer, B. Nagorny, and A. Hemmerich, Phys. Rev. A **67**, 051802 (2003).

[68] K. W. Murch, K. L. Moore, S. Gupta, and D. M. Stamper-Kurn, Nat. Phys. **4**, 561 (2008).

[69] F. Brennecke, S. Ritter, T. Donner, and T. Esslinger, Science **322**, 235 (2008).

[70] M. H. Schleier-Smith, I. D. Leroux, H. Zhang, M. A. Van Camp, and V. Vuletić, Phys. Rev. Lett. **107**, 143005 (2011).

[71] H. K. Cheung and C. K. Law, Phys. Rev. A **84**, 023812 (2011).

[72] J. D. Thompson, B. M. Zwickl, A. M. Jayich, F. Marquardt, S. M. Girvin, and J. G. E. Harris, Nature **452**, 72 (2008).

[73] U. Kemiktarak, M. Metcalfe, M. Durand, and J. Lawall, Appl. Phys. Lett. **100**, 061124 (2012).

[74] U. Kemiktarak, M. Durand, M. Metcalfe, and J. Lawall, New J. Phys. **14**, 125010 (2012).

[75] M. Pinard and A. Dantan, New J. Phys. **10**, 095012 (2008).

[76] J. Restrepo, J. Gabelli, C. Ciuti, and I. Favero, C.R. Phys. **12**, 860 (2011).

[77] C. H. Metzger and K. Karrai, Nature **432**, 1002 (2004).

[78] K. Usami, A. Naesby, T. Bagci, B. Melholt Nielsen, J. Liu, S. Stobbe, P. Lodahl, and E. S. Polzik, Nat. Phys. **8**, 168 (2012).

[79] A. Xuereb, K. Usami, A. Naesby, E. S. Polzik, and K. Hammerer, New J. Phys. **14**, 085024 (2012).

[80] D. J. Wilson, C. A. Regal, S. B. Papp, and H. J. Kimble, Phys. Rev. Lett. **103**, 207204 (2009).

[81] M. Karuza, M. Galassi, C. Biancofiore, C. Molinelli, R. Natali, P. Tombesi, G. Di Giuseppe, and D. Vitali, J. Opt. **15**, 025704 (2013).

[82] J. C. Sankey, C. Yang, B. M. Zwickl, A. M. Jayich, and J. G. E. Harris, Nat. Phys. **6**, 707 (2010).

[83] C. Biancofiore, M. Karuza, M. Galassi, R. Natali, P. Tombesi, G. Di Giuseppe, and D. Vitali, Phys. Rev. A **84**, 033814 (2011).

[84] A. Schilke, C. Zimmermann, P. W. Courteille, and W. Guerin, Phys. Rev. Lett. **106**, 223903 (2011).